Combined effect of multiple scattering and wind-driven sea waves on the results of sea water sensing using a lidar with a changeable field of view

G.P. Kokhanenko, M.M. Krekova, I.E. Penner, and V.S. Shamanaev

Institute of Atmospheric Optics,
Siberian Branch of the Russian Academy of Sciences, Tomsk

Received December 20, 1999

In this paper, we present the experimental data of seawater sensing using an airborne lidar with a changeable field of view, as well as the results of numerical simulations of the lidar operation by the Monte Carlo method. It is shown that the influence of sea waves leads to the increase of the rate of the return signal fall off with the increasing depth and to overestimation of the extinction coefficient measured at small field-of-view angles of the lidar receiver. Another cause of inefficient sensing with small field-of-view angles is strong fluctuations of the lidar return power, which cannot be described by normal distribution. At large field-of-view angles, multiple scattering partly compensates for the effect of sea waves. Applicability of simple models of the sea surface to description of the fluctuations of lidar return power is discussed.

Introduction

In recent years, we have compiled a large bulk of data on sensing seawater with a lidar mounted aboard a research vessel[1] or an aircraft.[2,3] Changes in the transparency of the upper 20-m seawater level were clearly revealed in these measurements, and inhomogeneities with horizontal scales from several to several hundreds kilometers were observed. The presence of such inhomogeneities forced us to consider again the problem on the accuracy of airborne lidar sensing. In this problem, we should take into account not only technical sources of errors, but also the physical ones associated with the water itself and with the influence of the water–atmosphere interface.

The parameters of recorded lidar returns (first of all, signal amplitude) undergo significant fluctuations even at a flight over the water surface sufficiently homogeneous along the horizontal direction. One of the known causes of this is the presence of specular glares arising as the laser beam hits a plane area normal to it. However, in the processing of lidar returns, a signal shape, rather than its absolute energy, is important. Thus, the most readily reconstructed optical parameter of the scattering media – the depth mean extinction coefficient of water – was determined from the signal fall off rate on the logarithmic scale.[2] Besides, it was confirmed that the measured extinction coefficient strongly depends on the receiver's field-of-view angle. This effect can be explained by the presence of multiply scattered radiation in the signal and it is observed in sensing clouds or dense aerosols also. Besides, the capabilities of extracting the information from lidar returns have been being widely discussed in recent time in the context of formation of multiple scattering at different lidar field-of-view angles.[4,5]

In the case of sensing of an aerosol or clouds in the atmosphere, the use of a minimal possible field of view (equal to the source divergence) guarantees the minimum contribution of multiply scattered radiation and, consequently, the best accuracy in reconstructing optical parameters of a medium. It is of course true only if the energy of a return signal is sufficient for its reliable recording. This is not the case with sensing of a hydrosol, since the presence of an irregular interface changes the temporal structure of a signal and introduces additional difficulties in the interpretation of lidar data.

Optical effects associated with the wind-driven waves on the sea surface have been studied for a long time and generalized in the well-known books.[6,7] In experiments[8] it was found that the absolute value of a return signal correlates with the state of the sea surface (surface rise at the sensing point). Many papers presented analysis and mathematical simulation of radiation propagation through the sea surface. The main attention was paid in them[9,10] to the presentation of a wave as an analog of a phase screen causing the well known amplification of backscattering as a wave twice passes the same inhomogeneities. This effect was described for the first time in Ref. 11 for the case of radiation propagation through a random scattering medium. In some limiting cases (regular waves, narrow beam as compared to the size of a surface wave), it was proposed to consider an illuminated area of the surface as a lens causing radiation focusing at some depth,[12–14,18,19] what may result in a strong distortion of the return signal. References 15 and 16 reported observations of such distortions (as irregular spikes in the depth behavior of the signal). Vlasov et al.[16] even argued that the amplification of backscattering almost completely masks signals from the underwater scattering layers.

The experience shows that the proposed models not always can satisfactorily explain signal distortions

0235-6880/00/04 337-11 $02.00

observed in actual experiments. This is connected not only with the approximate description of the surface in models, but also with the necessity of taking into account the geometric parameters of a lidar and among them the field-of-view angle, distance to the water surface, diameter of a receiving objective, and others. It is always a problem to consider these parameters in analytical approximations. The progress here is mostly associated with the development of statistical simulation (Monte Carlo method), which allows the optical and geometric conditions of an experiment to be taken into account more accurately than within the framework of the small-angle approximation[12,13,17] and the contribution of multiple scattering to be estimated. The use of the Monte Carlo method in the problems of water sensing[20,21] allowed the main peculiarities in the formation of multiple scattering to be revealed at different values of the lidar field-of-view angles for the case of a plane interface.

The algorithms of numerical simulation of a lidar return under conditions of wind-driven waves were proposed in Ref. 22. These algorithms enable one to estimate average (over space or an ensemble of realizations) radiation power. In Ref. 23 the formation of a lidar return was analyzed in detail based on the facet model of the surface, and the dependence of different-multiplicity scattering energy on wind velocity and receiver's field of view was obtained. In this paper, the algorithm is applied to estimation of distortions introduced by wind-driven waves in the measured extinction coefficient of water (that is, the rate of signal fall off with the increasing depth) at different lidar field-of-view angles. Thus, we have managed to compare the numerical and analytical methods of estimating the effect of sea waves with the results of field observations. The emphasis in this paper is placed on analysis of experimental data obtained in sensing with different lidar field-of-view (FOV) angles. The FOV dependence of the measured extinction coefficient mostly confirms the calculated results. Some peculiarities in the distribution of fluctuations of the lidar return power, which cannot be described within the framework of the facet model but hamper the operation of lidars with narrow FOV, are considered.

1. Experimental observations of lidar returns

1.1. Errors of lidar measurements and peculiarities of determination of the extinction coefficient in the upper layer of water

The seawater sensing experiments, the results of which are given below, were conducted in November 1996 over the Lake Baikal[2] and in June 1997 near Scotland.[3] In both of these cases, sensing was conducted from onboard an aircraft flying at the altitude of 200 m over the water surface. The lidar employed included a telescope of 150-mm diameter and a Nd:YAG laser emitting at the wavelength of 0.53 μm with the pulse output power of 50 mJ and the pulse repetition frequency up to 25 Hz. The full field-of-view angle $2\varphi_d$ ranged from 1.3 to 13 mrad. The lidar returns were digitized with a 7-bit analog-to-digital converter (ADC) at the quantization frequency of 120 MHz (this frequency corresponds to the depth resolution of 0.9 m).

Normally the lidar was operated at the pulse repetition rate of 5 Hz. The data were stored in files of 600 pulses each, what corresponded to the flight route length of 10 km. For every pulse, the depth range Δh was separated, inside which the return power was within the ADC dynamic range, and the depth mean extinction coefficient ε was calculated from the slope of the signal power function $\ln P(h)$ by the least-square method. A detailed description of the algorithms used can be found in Ref. 2. Besides the mean extinction coefficient ε, the method of least squares allowed us to estimate the error of calculation of the slope of each pulse (and, consequently, the error $\delta\varepsilon$ of calculation of the extinction coefficient) with regard for the well known properties of the linear regression.[24] This error depends on the error of signal power measurements at selected depths and on the number of readouts with the interval Δh. In a medium that is more turbid, as ε grew, the rate of the signal fall off with the increasing depth increased and the sensing interval Δh decreased (from $\Delta h = 12$ m at $\varepsilon = 0.15$ m^{-1} to $\Delta h = 4$ m at $\varepsilon = 0.4$ m^{-1}). As a result, the measurement error $\delta\varepsilon$ increased. This is especially true to life when analyzing records for which the extinction coefficient changed fast within one file. A linear regression was observed between $\delta\varepsilon$ and the extinction coefficient ε: $\delta\varepsilon = (0.1 \pm 0.04)\,\varepsilon$, and the regression coefficient was independent of the field of view within $2\varphi_d = 5 - 13$ mrad. (The error increased markedly at the minimum value of the field-of-view angle.) In other words, the relative error of measurement of the extinction coefficient $\delta\varepsilon/\varepsilon$ was within 10–15%.

For each file we calculated the mean value $\langle\varepsilon\rangle$ and the rms deviation $\Delta\varepsilon$. Comparison of the observed deviation $\Delta\varepsilon$ with the calculated error $\delta\varepsilon$ allows us to determine whether the spread in values of the extinction coefficient is caused by actual changes of water properties or it is a consequence of the measurement errors. For example, $\Delta\varepsilon$ was 0.6–0.8 of file-averaged $\delta\varepsilon$ at most homogeneous sections.

As was already mentioned, to estimate the extinction coefficient, one does not need to know the absolute power of a lidar return. However, the study of signal power fluctuations at different depths is interesting itself as applied to estimation of the characteristics of wind-driven waves.[17] As in the case of measurement of spatial inhomogeneities of the extinction coefficient, for this problem to be solved, the instrumentation used should allow separation of fluctuations of lidar return power against the background of fluctuations due to the instrumental noise.

The errors in a lidar measuring system are mostly

caused by the errors of signal digitizing with an ADC and the noise of the photomultiplier tubes (PMT's). Some estimates of the accuracy of lidar sensing were obtained in Ref. 25. Within the framework of this paper, there is no need to analyze in detail the instrumental errors of our receiving system. Let us only note that the relative errors of power measurements in the middle of the detector's operating range (10–40 units of ADC) are within 12–15% in the case of sensing of only weakly turbid water ($\varepsilon = 0.12$ m^{-1}) and the increase up to 18–20% in turbid water ($\varepsilon = 0.36$ m^{-1}) because of the faster change of the signal at the ADC input. In this connection, it should be noted that the fine effects of depth distribution of fluctuations at the level below 10%, which were predicted in Ref. 17, could hardly be measured experimentally.

1.2. Experimental results

Let us consider now some examples of lidar returns recorded at different field-of-view angles of the receiving system. Figure 1*a* shows the results obtained in the case of sensing of clean and horizontally homogeneous water in the central part of the Lake Baikal (November 1996) at two different values of the full FOV angle: $2\varphi_d = 13$ mrad (curve *1*) and 1.3 mrad (curve *2*). The shape of the lidar return shown in Fig. 1*a* was obtained from averaging over 100 laser shots. To extend the dynamic range of the recording system, changeable neutral density optical filters were used. Figures at the curves indicate the values of ε reconstructed from the measured signals.

Note that the depth of visibility of the Secchi disk observed in this region of the lake often achieves $Z_d = 25–30$ m in long-term measurements (Refs. 33 and 34). This corresponds to $\varepsilon \approx 7/Z_d \approx 0.23 - 0.28$ m^{-1}. Certainly, the processing of the data with $2\varphi_d = 1.3$ mrad overestimates the extinction coefficient. The slope of the curves at the depth of more than 5 m differs most markedly.

Figure 1*b* illustrates the shape of lidar returns received in flights over the Atlantic Ocean to the west from Great Britain (June 1997). For processing, we have selected the region with horizontally homogeneous water. For 10 min, the aircraft several times circled over the area of 5 km in diameter. To exclude the influence of specular reflection from the surface, the sensing was conducted at a sighting angle of 5 to 7° to the vertical. The data for each FOV angle were averaged over 600 laser shots (120 s of flight). The maximum FOV angle shown in Fig. 1*b* was $2\varphi_d = 10.8$ mrad (curve *1*), and the minimum FOV angle was 2.8 mrad (curve *2*). The ratio between the reconstructed values of the extinction coefficient at the minimum and maximum FOVs was 1.7. Below it is shown that the same value comes from the calculations with the use of the facet model of the surface.

The calculated mean values of the extinction coefficient $\langle\varepsilon\rangle$ and the rms deviations $\Delta\varepsilon$ obtained in this flight over the series of 600 measurements are given in Table 1 for different FOVs. This table also gives the mean error $\langle\delta\varepsilon\rangle$ of calculation by the least squares method and the mean interval of the processing depths Δh.

Table 1. Extinction coefficients measured at different FOV angles

$2\varphi_d$, mrad	10.8	8	5.4	2.8
$\langle\varepsilon\rangle$, m^{-1}	0.23	0.27	0.29	0.38
$\Delta\varepsilon$, m^{-1}	0.02 (8.6%)	0.03 (11%)	0.035 (14%)	0.07 (18%)
$\langle\delta\varepsilon\rangle$, m^{-1}	0.023	0.027	0.033	0.065
Δh, m	9–16	7–13	6–12	5–11

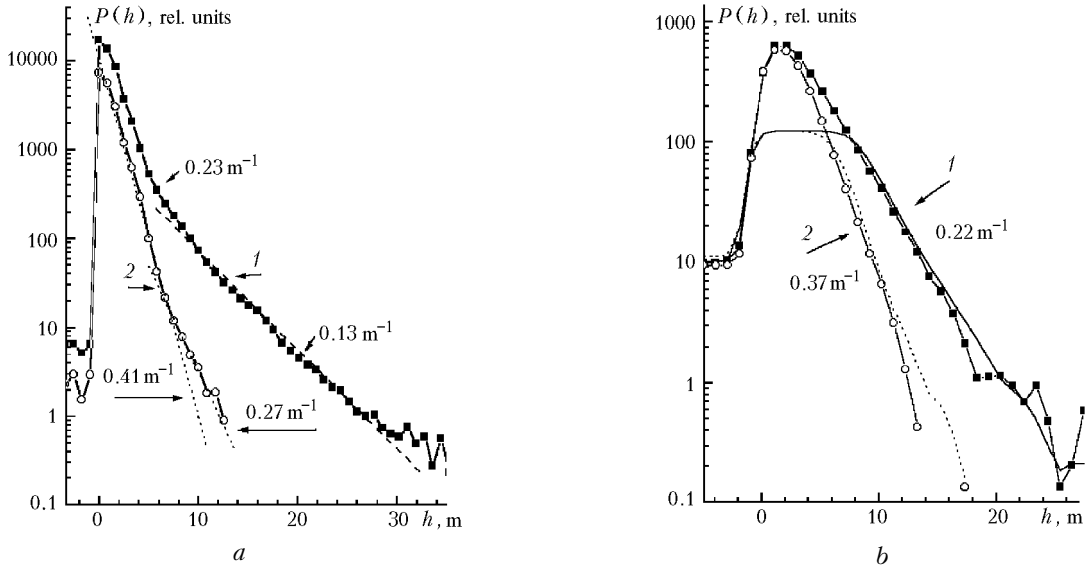

Fig. 1. Lidar signals obtained at different field-of-view angles: Lake Baikal, 1996, $2\varphi_d = 13$ (*1*) and 1.3 mrad (*2*) (*a*); Atlantic Ocean, 1997, $2\varphi_d = 10.8$ (*1*) and 2.8 mrad (*2*) (*b*).

One can see, first, that the spread $\Delta\varepsilon$ of the extinction coefficient values in a file is roughly equal to the calculated error of calculations, what also confirms the water homogeneity within the whole area under study. The measurements with the minimum FOV are characterized by not only the increase of the reconstructed value of ε, but also by the increase in the pulse-to-pulse spread of the results. The error of calculation of ε also increases because of the increasing fluctuations of the return signal power at all depths. The value of the return signal decreases at all depths with the decreasing FOV, and the distribution of the signal power changes: the data obtained with small FOV do not obey the Gaussian distribution. The histograms of distribution of the return signal power U from the depth of 10 m are shown in Fig. 2*a* (thin line in the figure shows the approximation by Gaussian distribution), and the parameters of distribution are given in Table 2. The mean pulse power $<U>$ decreases with the decreasing FOV, and the distribution mode shifts to the left. However, for all FOVs the number of high-power pulses distributed along the axis U up to the values more than 120 units of the ADC remains significant. As a consequence, at small FOV the parameters of the Gaussian distribution (U_0, σ), which most closely approximates the empirical distributions, differ widely from the mean $<U>$ and the rms deviation ΔU calculated for a series of 600 pulses. The data for the minimum FOV $2\varphi_d = 2.8$ mrad are characterized by a sharp growth of the amplitude of signal fluctuations (up to 190%) and by the shift (by more than two times) of the median with respect to the mean value.

Table 2. Parameters of signals from the depth of 10 m (see Fig. 2*a*)

$2\varphi_d$	10.8	5.4	2.8
Mean $<U>$ and rms deviation ΔU	42 ± 18 (43%)	15.6 ± 17 (110%)	6.7 ± 13 (190%)
Gauss: U_0, σ	36 ± 15	9.6 ± 4.5	2.7 ± 2.5
Median	37	10	3

Similar data but for the depth of 7.5 m are shown in Figs. 2*b* and *c*. The nearly Gaussian distribution is observed at $2\varphi_d = 10.8$ mrad (Fig. 2*b*), the median and the mean almost coincide (for this case a 10 dB attenuator was introduced in the receiving system). For the minimum FOV, (Fig. 2*c*) almost 12% pulses exceeding the upper limit of the ADC (128 bits) are remaining in the data array. The distribution parameters in this case are the following: $<U> = 35$, median = 19, $\sigma = 38$ (108%).

Figure 3 shows the histograms of distribution of pulse power at different FOVs, while at close modal values U_0 (therefore, they are taken at different depths). For illustration, a portion of the axis $n(U)$ within $n = 0 - 2$ is given on an enlarged scale. Parameters of distribution are given in Table 3. One can see here that at the same width of the Gaussian distribution at a small field of view (Fig. 3*c*) the uniform distribution is observed for strong pulses, some of which even exceed the ADC detection range.

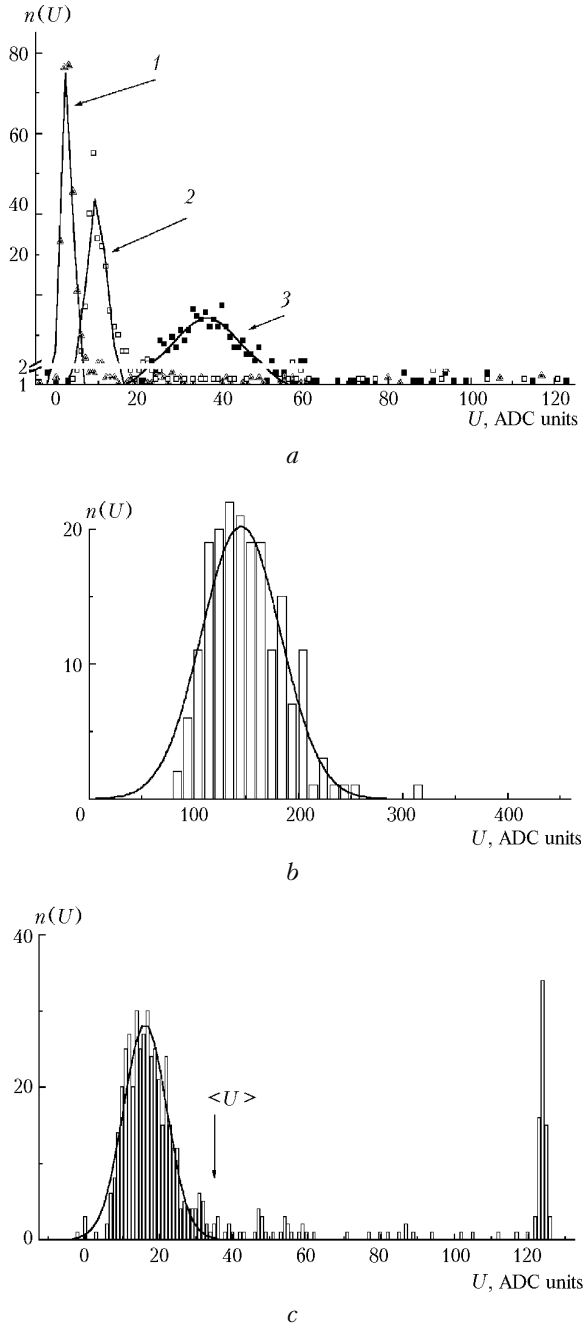

Fig. 2. Distribution of lidar signal power at different field-of-view angles: depth $h = 10$ m, $2\varphi_d = 2.8$ (*1*), 5.4 (*2*), and 10.8 mrad (*3*) (*a*); $h = 7.5$ m, $2\varphi_d = 10.8$ mrad (*b*); $h = 7.5$ m, $2\varphi_d = 2.8$ mrad (*c*).

Table 3. Parameters of signals shown in Fig. 3

$2\varphi_d$	(*a*) 10.8	(*b*) 5.4	(*c*) 2.8
Depth h, m	13	10	8
Mean $<U>$ and deviation ΔU	11 ± 3.4	15.6 ± 17	22 ± 34
Gauss: U_0, σ	10.8 ± 2.1	9.6 ± 4.5	7.7 ± 2.3

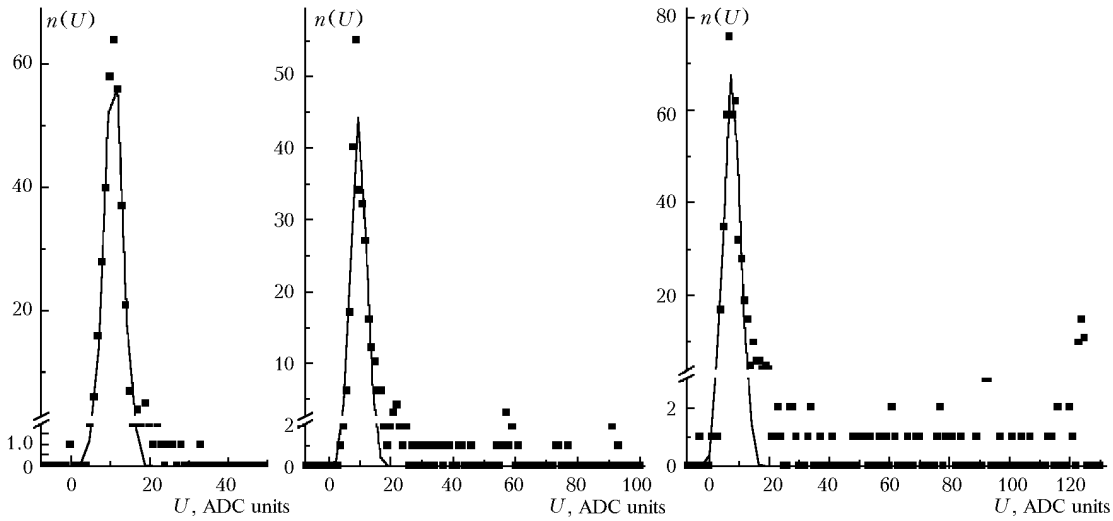

Fig. 3. Distribution of lidar return power at different field-of-view angles: $2\varphi_d$ = 10.8 mrad, h = 13 m (*a*); $2\varphi_d$ = 5.4 mrad, h = 10 m (*b*); $2\varphi_d$ = 2.8 mrad, h = 8 m (*c*).

A similar distribution, but at small depth is observed at a large field of view as well. It can be concluded that the normal distribution of amplitudes (when the mean $<U>$ coincides with the maximum U_0 for the Gaussian approximation) is observed only starting from some depth at a sufficiently low power: for the depth of 7 m at $2\varphi_d$ = 10.8 mrad and for 11 m at $2\varphi_d$ = 5.4 mrad. Even at a largest FOV the level of fluctuations almost twice exceeds the errors of signal power measurements. At smaller depths, the number of pulses whose power exceeds that given by the normal distribution increases. For the minimum FOV the normal distribution is not observed even for maximum depths. At the same time, analysis of the extinction coefficient for separate pulses at any FOV shows that there is no correlation between ε and pulse energy.

Let us make a tentative conclusion from the obtained results. It is clear that the systematic underestimation of the extinction coefficient in measurements with large FOV is caused by the influence of multiple light scattering. However, measurements with as small as possible FOV (equal to the laser beam divergence) undoubtedly give far overestimated values of ε. Moreover, the very wide spread in power of received signals, which sometimes exceeds the ADC dynamic range, makes such measurements little informative, since the depth a signal from which falls within the detector's dynamic range changes from pulse to pulse. This does not allow us to average the recorded signal along the flight route and thus to increase the measurement accuracy. Our experience in sensing shows that stable and repeatable results are achieved with a FOV no less than 6 mrad. The most probable cause of such a behavior of return signals is the effect of sea waves.

2. Analysis of the influence of sea waves on lidar measurements

Let us note first that we never observed irregular spikes in the depth profile of a signal, which were described in Refs. 15 and 16 as significantly exceeding the measurement errors and not related to the underwater inhomogeneities, although the time resolution of our photodetectors was higher than that in Ref. 15. The observed fluctuations were characterized by the sufficiently evenly increasing or decreasing signal level from pulse to pulse over the whole depth, what is supported by the already mentioned absence of correlation between the depth mean value of ε and $<U>$, as well as the relatively small variance of $\Delta\varepsilon$ fluctuations as compared with the variance of fluctuations of the signal power. Note that overestimation of the mean signal $<U>$ by about two times as compared with the mode (and median) of the distribution $n(U)$ at small FOV can be interpreted as manifestation of the effect of backscattering amplification, which must be observed only within small angles with respect to the backward direction.[10,11] However, already in Ref. 11 it was noted that the amplification effect may be relative rather than absolute. In our case, this means that the mean intensity in the backward direction increases as compared with the scattering in the lateral directions, but not with the case of a plane surface. The main effect associated with the random slope of a surface and leading to significant underestimation of the mean intensity at small FOV will be considered below.

2.1. Formation of echo signal at intersection of the "atmosphere – sea" interface

In this paper we analyze the influence of the air-water interface on the lidar return signals based on the facet model,[6,26,27] which considers the surface as a set of randomly oriented small surface elements with centers at the same plane $r = H$. The beam interacts with a surface element according to known Fresnel laws of reflection and refraction. To justify the applied algorithm, let us consider a specific scheme of airborne sensing of the sea.

Sensing is conducted along nadir from an aircraft flying at an altitude of 200 m over the surface. The total beam divergence angle is $2\varphi_s = 1.3$ mrad, so we see an illuminated spot $r_s = 0.13$ m in radius on the surface. Within a spot there are many capillary ($\lambda < 4$ mm) and gravitation-capillary ($\lambda < 7$ cm) sea waves.[6] The area of the observed surface (determined by the field of view of the receiving telescope), hydrosol-scattered radiation from which can be collected by the receiver, is even larger. This allows us to neglect any correlation between slopes of surface elements at the points of radiation entrance into the water and exit of scattered radiation from water when calculating the **mean** energy of a return signal. (In Refs. 29 and 30 it was shown that the effects of shadowing of waves and re-reflection of radiation between them should be taken into account only at grazing angles of sensing.)

In accordance with the facet model, the normals to the surface elements $S = (S_x, S_y, S_z)$ obey the normal distribution

$$P(S) = P(\alpha_x, \alpha_y) = \frac{1}{2\pi\sigma_x\,\sigma_y} \exp\left\{-\frac{\alpha_x^2}{2\sigma_x^2} - \frac{\alpha_y^2}{2\sigma_y^2}\right\}, \quad (1)$$

where $\alpha_x = S_x/S_z$, $\alpha_y = S_y/S_z$. The variance of the slopes depends on the wind velocity W. Usually, the dependence

$$\sigma_x^2 = 0.0031\ W, \quad \sigma_y^2 = 0.003 + 0.00192\ W \quad (2)$$

obtained in Ref. 26 is used. Reference 28 gives somewhat different dependence of σ^2 on the wind speed (obtained from the results of measurements in the Black Sea), which, however, shows that the empirical distributions obey the normal law. Besides, it is characteristic that the surface does not become plane ($\sigma^2 \neq 0$) even in the absence of wind. The rms slope of the surface elements in the absence of wind is $\sigma_W \approx 54$ mrad (3°) according to both Ref. 26 and Ref. 28. For our estimates we take the wind speed $W = 3$ m/s, at which the sea waves become almost isotropic with $\sigma_W = (\sigma_x\sigma_y)^{1/2} \approx$ ≈ 95 mrad according to Eq. (2).

If the beam is incident on a surface area inclined at an angle $\sigma_W = 95$ mrad to the vertical, then the beam deflection from the vertical above the sea surface is $\sigma_W(m - 1)/m \approx 24$ mrad ($m = 1.34$ is the refractive index of water). This exceeds the divergence angle of the laser beam and the field-of-view angle of our lidar by an order of magnitude. Conversely, a ray coming from underwater to the surface at this angle can fall within the telescope's field of view at an appropriate slope of the surface element. This casts some doubt on the utility of selection of minimum lidar fields of view in order to decrease the effect of multiple scattering.

Figure 4*a* shows the geometry of formation of a single scattered return signal for the plane interface. Here H is the distance to the interface, h in the depth in water; R is the radius of the receiving objective. Let us write the lidar equation for the case of single scattering in a simplified form:

$$P(h) = C\Omega\sigma_\pi(h) \exp(-2\tau), \quad (3)$$

where C is the calibration constant; τ is the optical thickness of the path; σ_π is the backscattering coefficient; Ω is the solid angle of the cone of single scattered radiation coming to the receiver (in other words, the angle at which the receiver is seen from the point of the light scattering event). For a plane surface as well as for a homogeneous medium, single scattered radiation can come to the receiver only from the area of the laser spot (circle of radius r_s in Fig. 4*a*). However, the angle θ at the cone vertex within which the single scattered radiation that reaches the receiver is far less than φ_s. For air this angle is equal to $\theta = R/(H + h)$. (Hereinafter, it is assumed that $\theta \ll 1$ because of the experimental geometry.)

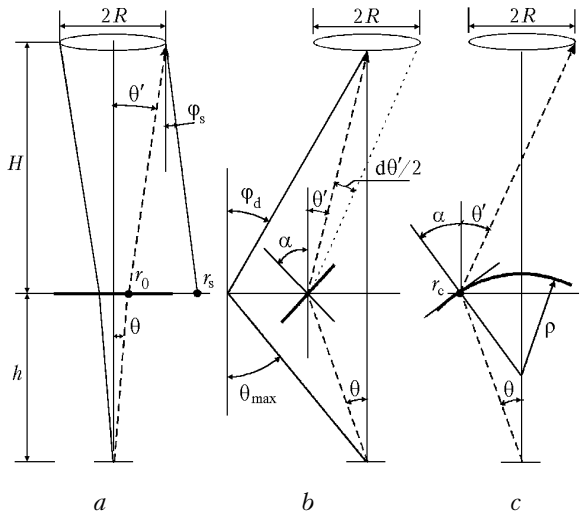

Fig. 4. The scheme of radiation passage through surface: plane surface (*a*), facet model (random slope of surface elements) (*b*), and spherical surface (*c*); φ_s is the beam divergence angle; φ_d is the field-of-view angle. The dashed line shows the ray scattered at an angle (180°−θ).

Taking into account that the angles of ray deflection in water θ and in air θ' are related as $\theta' = m\theta$, for the plane surface it is easy to obtain

$$\theta = R/(Hm + h), \quad \Omega_0(h) = \pi\theta^2. \quad (4)$$

This value is somewhat smaller than it is in the case of no interface in a homogeneous medium. For example, at the objective of the receiving telescope of $R = 0.1$ m in radius, the angle is $\theta = 0.35$ mrad at the depth of 20 m and the area of cone intersection with the surface has the radius $r_0 = 7$ mm. Several sea capillary waves are present along this length, and there is no full correlation of the surface slope at the entrance and exit points. Let us imagine that the ray coming strictly upward from underwater falls on a surface element with the slope σ_W. Then its deflection from the vertical in air is $\sigma_W(m - 1) \approx 32$ mrad, what is 100 times larger than the cone angle of the radiation coming to the receiver. Consequently, a significant part of single scattered radiation, which would fall in the receiver in the

case of a plane surface, does not fall in it in the case of a rough surface. On the other hand, since the mean slope of surface elements σ_W far exceeds the field-of-view angle, there are many surface elements, which deflect toward the desired direction a portion of single scattered radiation not coming to the receiver in the case of a plane surface. Therefore, the power of single scattered radiation increases with the increasing field of view and saturates (as was shown in Ref. 23) at the field of view about $\varphi_d \approx 1°$ at the level of 70% of the corresponding power in the case of a plane surface.

Let us consider (Fig. 4*b*) beam passage through a surface at a random slope of a surface element. Assume the angle θ in water to be given (backscattering at an angle of $180° - \theta$) and the axis X to lie in the scattering plane. Let the surface element be inclined at an angle $\alpha = (\alpha_x, \alpha_y)$. Using the relation between the angle of incidence $(\alpha - \theta)$ and the angle of refraction $(\alpha + \theta')$, one can easily obtain that the ray comes to the center of the receiver if the surface element is inclined at the angle

$$\begin{cases} \alpha_x = \dfrac{(Hm + h)}{H\,(m-1)}\,\theta \\ \alpha_y = 0 \end{cases}. \qquad (5)$$

The probability that the ray falls in the receiver is

$$E(\alpha) = \pi/4\; P(\alpha_x, \alpha_y)\; d\alpha_x\, d\alpha_y, \qquad (6)$$

where $P(\alpha)$ can be determined from Eq. (1), and $d\alpha$ is determined by the variability limits of the element slope at a fixed scattering angle θ, at which the ray is within the receiver. It can be shown that $d\alpha = d\theta'/(m-1)$, $d\theta' = 2R/H$, and, consequently, $d\alpha_x d\alpha_y = 4R^2/H^2(m-1)^2$.

Since the point at which the ray intersects the surface must be within the receiver's field-of-view angle φ_d, the scattering angle θ varies from 0 to $\theta_{max} = \varphi_d H/h$ (this is true at $\theta_{max} \ll 1$, what is the case at the depth $h = 20$ m even at the maximum lidar field-of-view angle). The power of single scattered radiation can be expressed as

$$P(h) = C \exp(-2\tau) \int_0^{\theta_{max}} \sigma(180° - \theta, h)\, E(\theta)\, \pi\theta\, d\theta \approx$$

$$\approx C \exp(-2\tau)\, \sigma_\pi(h)\, \Omega_F(h). \qquad (7)$$

In Eq. (7) it is additionally assumed that the scattering phase function is constant within the scattering angle $(180 - \theta_{max})$. In Eq. (7) Ω_F is the integral having the meaning of the effective solid scattering angle (cp. with Ω_0 in Eq. (1) for the plane surface).

Having substituted Eqs. (1), (5), and (6) into Eq. (7), and calculated the integral, we have for Ω_F:

$$\Omega_F = \frac{\pi R^2}{(Hm + h)^2}\left[1 - \exp\left(-\frac{(Hm-h)^2}{(m-1)^2 h^2}\,\frac{\varphi_d^2}{2\sigma_W^2}\right)\right] = K\Omega_0. \qquad (8)$$

The expression in brackets denoted as K determines the factor of underestimation of the signal power as compared with the case of the plane interface. The value of K depends significantly on the lidar FOV. At $\varphi_d > 5$ mrad $K \approx 1$, consequently, there is no power loss. As φ_d decreases, the losses increase (at the depth $h = 20$ m with $\varphi_d = 1.3$ mrad $K = 0.29$, and at $\varphi_d = 0.13$ mrad $K = 0.003$), and they also increase with the increasing depth. At $\varphi_d \ll 1$ (in fact, at $\varphi_d < 1$ mrad for $h > 20$ m) Eq. (8) simplifies significantly:

$$K \approx \frac{(Hm-h)^2}{(m-1)^2 h^2}\,\frac{\varphi_d^2}{2\sigma_W^2}. \qquad (9)$$

It is seen from Eq. (9) that at a small FOV extra [as compared with that given by Eq. (3)] extinction of the signal takes place, and this extinction is proportional to the squared depth. Consequently, the rate of the lidar return fall off increases, and this may be misinterpreted as the increase of the extinction coefficient ε of water. For example, in the depth range of 5 – 15 m, which is most convenient for processing of signals, the extra extinction of the signal by nine times corresponds to the increase of ε by 0.11 m^{-1}, what is comparable with the value of ε itself in transparent water. Calculation of the signal power by Eqs. (7) and (8) for the angle $\varphi_d = 0.13$ mrad (the case when multiple scattering is negligible) is shown in Fig. 5 as curve *8* (dashed line). It closely agrees with the numerical results obtained by the Monte Carlo method. Note that the curve $P(h)$ on this semi-logarithmic scale deviates from a straight line and becomes convex down. Just this shape of the return signal fall off was often observed in our field experiments (Fig. 1*a* and Ref. 1).

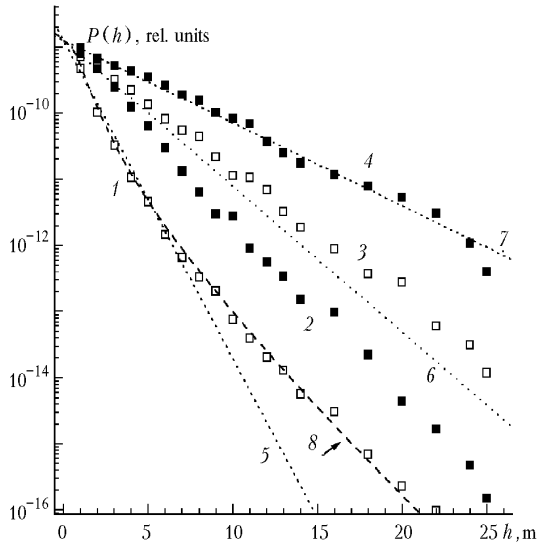

Fig. 5. Total lidar signal at different field-of-view angles: calculation for $2\varphi_d = 0.28$ (curve *1*), 1.08 (*2*), 2.8 (*3*), and 10.8 mrad (*4*). The dashed line shows the exponential dependence for $\varepsilon = 0.55$ (*5*), 0.25 (*6*), and 0.14 m^{-1} (*7*); calculation by Eq. (8) (curve *8*).

2.2. Numerical calculations

Analysis that more accurately considers the influence of sea waves on the measured value of the extinction coefficient with the allowance made for both single and multiple scattering can be obtained at numerical simulation of the lidar operation by the Monte Carlo method. Below we present the calculated results. In calculations of the lidar returns, we used the scheme of local estimation of the flux, which was described in detail in Ref. 23. We also used water optical parameters typical of open ocean: scattering phase function $g_1(\mu)$ calculated in Ref. 21 by the model of the particle spectrum of the Pacific ocean water,[32] mean cosine $<\cos\mu> = 0.95$, the probability of photon survival $\Lambda = 0.8$, and the extinction coefficient $\varepsilon = 0.25$ m^{-1}. The lidar parameters corresponded to actual values.

In Ref. 23 it was stated that the double intersection of the wavy surface causes fast extinction of signal components of low scattering orders at small FOV. Figure 6 shows the depth profiles of the components of different scattering orders in the lidar signal at different fields of view. The wind speed is taken to be $W = 3$ m/s, and the distance to the surface is 200 m. The depth in water is plotted along the horizontal axis, and the relative signal power is plotted along the vertical axis. The dashed line shows the depth profile of the single scattering signal in the case of a plane water surface: $P(h) \sim \exp(-2\varepsilon h)$. Figures at the curves indicate the scattering order; Σ is the total scattering signal.

Maximum losses of the signal are observed at the smallest FOV $\varphi_d = 0.134$ mrad (Fig. 6*a*). Not only the single scattering component, but also the total signal falls off faster than in the case of a plane surface. The single scattered radiation at $\varphi_d = 1.34$ mrad (Fig. 6*b*) falls off with the increasing depth faster than $\exp(-2\tau)$, but the contribution of multiple scattering exceeds that in the previous case, and the rate of the fall off of the total signal is close to that of $\exp(-2\tau)$. Finally, at $\varphi_d = 10.7$ mrad (Fig. 6*c*) the rate of the single scattering signal fall off is the same as for the plane surface, but the contribution of multiply scattered radiation prevails, and the rate of the fall off of the resulting signal is significantly lower. It is seen from Fig. 6 that the energy of single scattered radiation already does not concentrate within the field of view equal to the laser beam divergence $\varphi_d = \varphi_s$, but depends on the receiver's FOV. Formation of the single scattered radiation terminates at $\varphi_d \approx 1°$.

Figure 5 shows the total signal at different FOVs. The values of the scattering coefficient ε' reconstructed from the rate of the total signal fall off are significantly overestimated as compared with the actual value $\varepsilon = 0.25$ m^{-1} at small FOVs and underestimated at large FOVs. For only one value of FOV (namely, $\varphi_d = 1.34$ mrad) the influence of multiple scattering compensates for the influence of the wavy surface, and the reconstructed value of ε' coincides with the true value of ε. Besides, it is seen that the analytical approximation by Eqs. (7) and (8) agrees closely with the results of numerical calculations at small FOVs (cp. curves *8* and *1*).

The numerical calculations show that the wind speed in the chosen model of the surface (within 3–7 m/s) affects only the energy of the lidar return signal and does not change the slope of the curve $\ln P(h)$ [this follows from Eq. (9) as well]. The ratio between the reconstructed values of ε' measured at different (but not very small) FOVs depends mostly on the contribution of multiple scattering and turns out to be the same as in the case with a plane interface. For example, for the limiting FOVs in the experiment of 1997 ($2\varphi_{min} = 2.68$ mrad, $2\varphi_{max} = 10.8$ mrad), this ratio equals to 1.6. As could be seen earlier, it was just this value we observed in our experiments. The calculations also show that, as for the plane wave, the contribution from the components high orders of scattering is determined by the optical diameter of the field-of-view area on the surface $\eta = \varepsilon\, 2\varphi_d\, H$, rather than by the FOV angle φ_d itself. At the same time, distortion of the shape of single scattered signal [according to Eqs. (7) and (8)] is independent of the extinction coefficient ε.

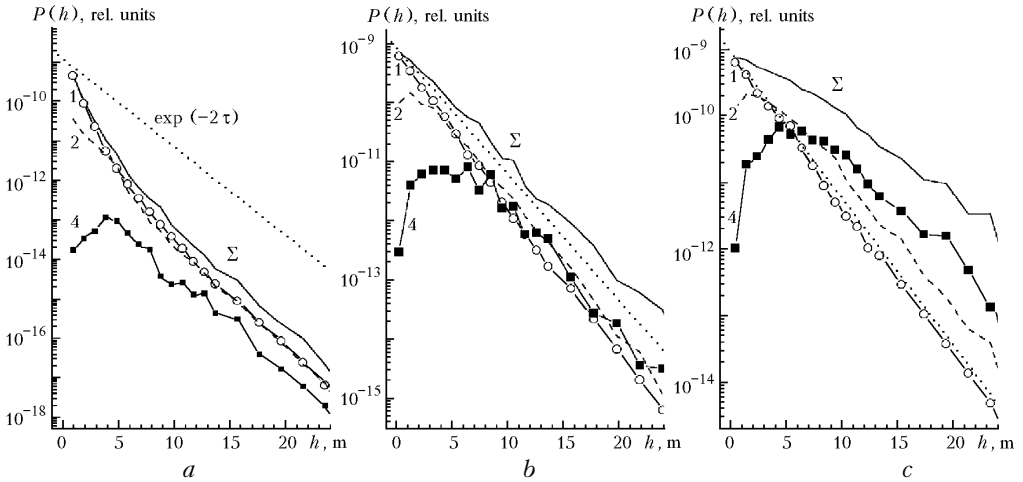

Fig. 6. Formation of components of different scattering orders at different lidar field-of-view angles; $2\varphi_d = 0.28$ (*a*), 2.8 (*b*), and 10.8 mrad (*c*).

2.3. Analysis of applicability of the facet model of surface to lidar sensing

The above analysis explains the main peculiarities of lidar returns and, in the first place, of the observed overestimation of the extinction coefficient at small lidar FOVs. At the same time, the character of the observed fluctuations of the lidar return power is not clear. Certainly, the earlier considered facet model of the sea surface must lead to the normal distribution of pulse amplitudes, since every signal is the result of radiation interaction with a large number of surface elements each having a random slope. Actually, at a small FOV fraction of signals with anomalously high energy is large. They are characterized by the same (on the average) rate of power decay with the increasing depth (and, consequently, the same value of ε'), but their energy is independent of the lidar field-of-view angle. Besides, our experience shows that the FOV, at which the contribution of multiple scattering and the influence of the surface compensate each other, is somewhat larger than the value estimated in our calculations $2\varphi_d = 2.68$ mrad.

As was already mentioned, we did not observe effects connected with radiation focusing at some depth and described by a "single-lens" model.[16,18] For these effects to exist, the size of the illuminated spot on the surface should be several times less than the wavelength of a surface wave. This case was demonstrated in the model experiments.[16] However, it was noted in Ref. 16 that ripples on the surface can fully mask the effect of large waves.

In the geometric-optics approximation, the decisive size is the size of the area of intersection of the single scattered radiation cone with the surface (r_0 in Fig. 4*a*), rather than the beam radius on the surface. In our sensing scheme, this size was $r_0 = 7$ mm. Even such value of the radius is sufficient for several capillary waves to be present along them, and there is a good reason to neglect the correlation of the surface slope at all the points of the radiation entrance and exit. This is just the circumstance that allows us to apply the facet model and believe that the outgoing radiation at any point of the surface deflects from the initial direction with equal probability. However, it is clear that as the radiation passes twice through the surface (for fractions of microseconds), the surface has no time to change its state. The radiation scattered strictly in the backward direction (180°) passes through the same point on the surface as at the entrance and comes back to the receiver at any state of the surface.

We can assume that there is some area of radius r_c around the point of ray entrance to the water, within which the surface can be considered as "frozen" for the single scattered radiation from underwater. The radiation having reached the surface within a circle of radius r_c arrives in the receiver without extinction, which was predicted in the facet model when calculating the mean characteristics of the signal. The size r_c of the area depends both on the correlation length of the sea waves, which is about one fourth of the wavelength of a surface wave,[17] and on the surface curvature at the entrance point. In practice, the correlation length of the sea waves can hardly be estimated, since the surface is a set of waves of different lengths, and the situation changes from pulse to pulse. Let us consider now how the surface curvature affects r_c.

The geometry of ray passage through the spherical surface is shown in Fig. 4*c*. The angle θ determines what rays fall on the receiver edge. It intersects the surface at the distance r_c from the vertical. The radius of surface curvature ρ determines its slope α at this point. Assuming, that the sensing depth far exceeds the radius of curvature ($h \gg \rho$), we can derive the equation for the solid angle of the cone of single scattered radiation

$$\Omega_c = \frac{\pi R^2}{(m-1)^2 H^2} \frac{\rho^2}{h^2}. \qquad (10)$$

In this case, the radius $r_c = R\rho/(m-1)H$ is independent of the depth (in contrast to a plane surface). By comparing Eqs. (10) and (4), we can see that the extra extinction introduced by the spherical surface does not depend on the receiver's field of view, though has the same depth dependence as in the facet model (9). This explains the fact that the experimentally observed rate of signal fall off with the increasing depth is independent of the pulse energy, and the energy of anomalously high-power pulses is independent of the lidar's field of view.

At the same time, to estimate the contribution of the "frozen" radiation to the total signal energy, one needs to estimate correctly the mean curvature radius. From Ref. 31 we know the experimental measurements of the curvature of surface elements at different wind velocity, which were obtained by observing specular flares from an artificial light source. According to these estimates, the radius of curvature ranges from 14 to 25 cm. This results in the value of r_c about 0.3 mm and the negligibly small energy of the "frozen" part of the signal (10). This energy is almost three orders of magnitude lower than that for a plane surface and far lower than the facet-model estimate of the mean energy attenuated by sea waves. Therefore, the major part of return signals do not show evidence of freezing, and in the distribution $n(U)$ (for example, in Fig. 2*c*) they are shown as a compact group with the almost Gaussian distribution.

At the same time, a significant part of the surface can have very small curvature (of any sign) in at least one direction, and such areas could not be taken into account in Ref. 31 because of the measurement technique chosen. This is especially true for capillary waves, which are characterized by wide ridges and sharp hollows.[6] The energy (10) of frozen pulses increases fast with the increasing radius of curvature ρ. Since for every laser pulse the value of r_c is obtained by averaging over the area illuminated by the laser beam,

the mean values of r_c cannot exceed the correlation length of sea waves. For example, if we take r_c to be equal to one fourth of the maximum wavelength of capillary waves (r_c = 1 mm), then for φ_d = 0.13 mrad and h = 20 m the power of the frozen part (10) is six times higher than that calculated using the facet model (9). The energies of the recorded pulses in Fig. 2*c* are distributed within roughly the same limits. Since every laser pulse interacts with its own pattern of the wavy surface, r_c can vary widely, what explains the almost uniform character of the experimentally observed distribution of the energy of high-power pulses.

The power of the frozen part of the return signal can achieve the full power of the return signal in the case of a plane surface, if $r_c \geq r_0$ at a given sensing depth. This is more likely in the upper water layers, where r_0 is small, and just there we observe a significant number of pulses with anomalously high power. With the increasing depth, r_0 grows and the relative part of the frozen radiation decreases. At a large field of view, at which the contribution of multiple scattering is significant and energy underestimation in the facet model is low, on the average, this part becomes insignificant, whereas it is significant at a small field of view.

The observed pattern also depends on the lidar position over the surface. In the case of the low (shipborne) position of the receiver, the angle Ω_0, at which the receiver is seen, is large, and r_0 is far longer than the wavelength of sea waves and part of the frozen radiation is small. The measurements[1] conducted in such a situation with a lidar having large FOVs (10 mrad) show that in this case signal power fluctuations are the same all over the depth, achieve the level of 30%, and have the normal distribution.

The above consideration of the "frozen" interface describes the effect similar, in a certain sense, to the backscattering amplification at double passage of a phase screen. This is possibly the consideration, from the viewpoint of geometric optics, of the same mechanism of radiation interaction with a surface, since in both approaches the correlation length of waves is the characteristic size. However, this approach allowed us to use the parameters of an actual lidar experiment (receiver size, field of view, etc.) for estimates and showed that the effect we observed in practice is not amplification of backscattering, but a weaker extinction of some return signals than that predicted by the facet model. The obtained estimates of the possible spread in energies of individual pulses are qualitatively confirmed by the results of field experiments.

Conclusion

In this paper, we considered the effects associated with lidar sensing of the upper sea layer: multiple scattering and sea roughness. These effects have opposite influence on the measured extinction coefficient. The effect of the sea roughness results in that the power of single scattered radiation falls off faster with the increasing depth than the exponential function, and the measured extinction coefficient in water proves to be overestimated. Conversely, multiple scattering decreases the fall off rate of the return signal. At certain FOV angles these effects compensate for each other, and the extinction coefficient calculated from the signal fall off rate coincides with its actual value. The calculations by the Monte Carlo method using the facet model of the rough sea surface give the value $2\varphi_d \approx 2.6$ mrad for such a FOV.

However, it follows from the experimental data that at this FOV the obtained values of ε are somewhat overestimated. Sensing of water with such a small FOV is very inefficient because of strong power fluctuations of the return signals, which are not described by the normal distribution. The interval of depths, within which the lidar return falls within the detector's dynamic range, changes from pulse to pulse. This hampers spatial (along the flight line) averaging of lidar returns and calculated optical characteristics of water and leads to an increase of the error in the extinction coefficient.

According to calculations, formation of single scattered radiation terminates at $2\varphi_d \approx 10$ mrad. The experimental data show that as the FOV increases up to $2\varphi_d \approx 8$–10 mrad, power fluctuations of the lidar return signals decrease significantly and their distribution approaches the Gaussian one. These angles are optimal for sensing, although one should take into account that the reconstructed value of the extinction coefficient may be somewhat underestimated because of the effect of multiple scattering.

The causes for appearance of anomalously high-power return signals at small FOV are discussed. The state of the frozen interface is considered, in which a part of single scattered radiation enclosed in a cone with an acute angle in the direction of 180° passes through the same surface element as in the first downward passage. The estimate shows that the energy of some pulses may exceed the mean energy by almost an order of magnitude. The mean signal $<U>$ at small FOV is overestimated roughly twice as compared with the distribution mode $n(U)$. This overestimation can be interpreted as a manifestation of the well known effect of the backscattering amplification.

Power fluctuations of the return signals at any FOV and at all depths far exceed the measurement error. This gives grounds for planning experiments on studying the dependence of the variance of fluctuations on the characteristics of sea waves.

References

1. G.P. Kokhanenko, I.E. Penner, and V.S. Shamanaev, Atmos. Oceanic Opt. **11**, No. 7, 614–620 (1998).
2. G.P. Kokhanenko, I.E. Penner, V.S. Shamanaev, G. Ludbrook, and A. Scott, Atmos. Oceanic Opt. **12**, No. 1, 37–43 (1999).
3. G. Kokhanenko, I. Penner, V. Shamanaev, G. Ludbrook,

and A. Scott, in: *13th Annual Int. Symp. on AeroSense*, Orlando, Florida, USA (1999).
4. V.V. Veretennikov, Atmos. Oceanic Opt. **12**, No. 5, 369–375 (1999).
5. L.R. Bissonnette and D.L. Hutt, Appl. Opt. **34**, No. 30, 6959–6975 (1995).
6. A.S. Monin and P.P. Krasnitskii, *Phenomena on Ocean Surface* (Gidrometeoizdat, Leningrad, 1985), 374 pp.
7. V.N. Pelevin, in: *Ocean Optics*. Part 2. *Applied Ocean Optics*, ed. by. D.S. Monin (Nauka, Moscow, 1983), pp. 101–111.
8. F. Hoge and R. Swift, Appl. Opt. **22**, No. 1, 37 (1983).
9. Yu.B. Dorofeev and A.G. Luchinin, in: *Sea Optics*, ed. by K.S. Shifrin (Nauka, Moscow, 1983), pp. 154–158.
10. A.G. Luchinin, Izv. Akad. Nauk SSSR, Ser. Fiz. Atmos. Okeana **15**, No. 7, 770–775 (1979).
11. A.G. Vinogradov, Yu.A. Kravtsov, and V.I. Tatatrskii, Izv. Vyssh. Uchebn. Zaved., Ser. Radiofiz. **16**, No. 7, 1064–1070 (1973).
12. L.A. Apresyan and D.V. Vlasov, Atmos. Oceanic Opt. **5**, No. 1, 1–7 (1992).
13. V.L. Veber and I.A. Sergievskaya, Izv. Ros. Akad. Nauk, Ser. Fiz. Atmos. Okeana **28**, No. 3, 325–333 (1992).
14. J.W. McLean and J.D. Freeman, Appl. Opt. **3**, No. 18, 3261–3269.
15. D.V. Vlasov, Izv. Akad. Nauk SSSR, Ser. Fiz. **49**, No. 3, 433 (1985).
16. D.V. Vlasov, V.N. Streltsov, and V.P. Slobodyanin, in: Trudy IOFAN, Vol. 1, *Remote Sensing of Ocean*, ed. by A.M. Prokhorov (Nauka, Moscow), pp. 39–59.
17. A.G. Luchinin, Izv. Akad. Nauk SSSR, Ser. Fiz. Atmos. Okeana **34**, No. 5, 686–692 (1998).
18. V.L. Veber, in: *Atmospheric and Sea Optics. Abstracts of Reports* (GOI, Leningrad, 1988), pp. 406–407.
19. S. Babichenko, A. Dudelzak, and K. Saar, Izv. Akad. Nauk Eston. SSR, Ser. Fiz.–Matem. **36**, No. 3, 319–322 (1987).
20. G.M. Krekov, M.M. Krekova, and I.V. Samokhvalov, Issled. Zemli iz Kosmosa, No. 6, 77 (1986).
21. G.M. Krekov and M.M. Krekova, Atm. Opt. **2**, No. 1, 55–61 (1989).
22. E.O. Dzhetybaev and B.A. Kargin, in: *Urgent Problems of Applied Mathematics and Mathematical Simulation* (Nauka, Novosibirsk, 1982), pp. 83.
23. B.A. Kargin, G.M. Krekov, and M.M. Krekova, Atmos. Oceanic Opt. **5**, No. 3, 191–195 (1992).
24. B.R. Levin, *Theoretical Principles of Statistical Radio Engineering* (Sov. Radio, Moscow, 1969), 741 pp.
25. I.E. Penner and V.S. Shamanaev, Opt. Atm. **1**, No. 7, 84–90 (1988).
26. G. Cox and W. Munk, J. Opt. Soc. Am. **44**, 833–850 (1954).
27. Yu.A.R. Mullamaa, Izv. Akad. Nauk SSSR, Ser. Fiz. Atmos. Okeana **4**, No. 7, 770–775 (1968).
28. V.N. Pelevin and Yu.G. Burtsev, in: *Optical Studies in Ocean and in the Atmosphere above Ocean* (IO AN SSSR, Moscow, 1975), pp. 202–220.
29. B.A. Kargin, in: *Mathematical Problems of Geophysics* (Novosibirsk, 1983), pp. 25–40.
30. K.B. Rakimgulov, "*Statistical simulation of the field of optical radiation in the system ocean–atmosphere*," Author's Abstract of Doctor's Thesis (Novosibirsk, 1993).
31. Yu.A. Burtsev and V.N. Pelevin, in: *Light Fields in Ocean* (IO AN SSSR, Moscow, 1979), pp. 231–232.
32. O.V. Kopelevich, in: *Ocean Optics*. Vol. 1, *Physical Ocean Optics* (Nauka, Moscow, 1983), pp. 208–235.
33. P.P. Sherstyankin, in: *Optical Methods of Study of Oceans and In-land Water Areas* (Nauka, Novosibirsk, 1979), pp. 16–27.
34. P.P. Sherstyankin, in: *Physical Limnology of Lake Baikal: a Review*, ed. by M.N. Shimaraev and S. Okuda (Baikal International Center for Ecological Research, Irkutsk–Okayama, 1994), pp. 24–30.